Volume 53, issue 1, January 2012   ISSN 0196-8904

ELSEVIER

ENERGY
Conversion and Management
An International Journal

Editor-in-Chief: Dr Jesse Denton
Editors: Dr Sümer Şahin
        Dr Mohamed Al-Nimr

- Energy Conversion Systems
- Magnetohydrodynamics
- Biological Conversion
- Energy Management and Conversion
- Direct Energy Conversion
- Energy Storage
- Alternative Energy Systems
- Thermal Energy Conversion and Power

Available online at www.sciencedirect.com
SciVerse ScienceDirect

(This is a sample cover image for this issue. The actual cover is not yet available at this time.)

Recuperative solar-driven multi-step gas turbine power plants

S. Sánchez-Orgaz [a], A. Medina [b,*], A. Calvo Hernández [b,c]

[a] *Departamento de Física, Ingeniería y Radiología Médica, ETSII de Béjar, 37700 Béjar, Salamanca, Spain*
[b] *Departamento de Física Aplicada, Universidad de Salamanca, 37008 Salamanca, Spain*
[c] *IUFFYM, Universidad de Salamanca, 37008 Salamanca, Spain*

ABSTRACT

An analysis on the influence of the recuperator effectiveness in a multi-step solar-driven Brayton engine is presented. The solar collector model includes heat losses from convection and radiation. The Brayton engine includes an arbitrary number of turbines and compressors, regeneration, and several realistic irreversibility sources. It is stated that the combination of both systems makes the evolution of the overall efficiency with the effectiveness of the regenerator not trivial. Such behavior is associated to the losses arising from the coupling of the working fluid with the collector and the surroundings. The overall efficiency admits a simultaneous optimization in regards to the pressure and temperature ratios. When the system is designed to work close to the optimum values of those parameters an increase in the effectiveness of the recuperator is always associated with an increase in the overall optimum efficiency. This holds for configurations from the simplest solarized Brayton up to arrangements with several turbines and compressors.

1. Introduction

The use of regeneration, in combination with intercooling and reheating, in gas turbine power plants is a key concept in order to improve efficiency and reduce fuel consumption by introducing a heat exchanger that transfers waste heat exhausted from the turbine to preheat air from the compressor. Additionally, when the sun energy is used to drive the gas turbine the main advantage of the recuperator is the preheating of the working fluid before the receiver. This leads to a reduction of the surface of the concentration system and then to a saving of investment and maintenance costs.

Solarized and recuperative stand-alone gas turbine power plants or in combination with a bottoming Rankine cycle, have been proposed as a real possibility in the development of efficient installations with significant cost reductions for solar electric power generation [1–6]. These plants use direct solar heating of pressurized air by means of central receiver technology to get working temperatures over 1100 °C [7,8]. The feasibility of gas turbines to operate in a solar-fossil hybrid way has been also proved by means of appropriate combustion chambers [1,3–5], thus allowing predictable performance even when little or no solar energy is available.

From a theoretical point of view different results have been reported for solar-driven Carnot-like models with external [9–12]

and internal [13–16] irreversibilities, for Braysson [15,17,18], Ericsson [19], and Rankine [20,21] cycle models under different optimization criteria. However, for solar-driven gas turbine cycles the reported analytical results are quite scarce: they include works for regenerative [22–24] and non-regenerative solar cycle models with one turbine-one compressor standing alone [15,25] or in combination with steam cycles [26]. Together with regeneration, multi-step compression and expansion constitutes a direct way to improve the thermal efficiency of the plant, although with the consequent cost increase. An economical analysis becomes necessary in order to balance the increment on efficiency with respect to the increase of costs.

The main purpose of this paper is to present a detailed theoretical analysis on the influence of the regenerator effectiveness in a multi-step, solarized Brayton cycle model which incorporates the main irreversibility sources, both for the thermal engine itself as for the solar collector. For the concentrating collector we assume a model which accounts for radiative and convective losses [18,27,28]. For the thermal Brayton cycle we assume a regenerative multi-step Brayton heat engine model with an arbitrary number of turbines N_t and compressors N_c accounting for: the non-ideal behavior of turbines and compressors, pressure drops during the heat input and heat release stages, regenerator irreversibility, heat leakage through the plant to the surroundings, and non-ideal couplings of the working fluid with the external heat reservoirs [29,30].

Although our numerical model allows for the consideration of an arbitrary number of turbines and compressors the main focus will be on realistic, recuperative configurations ranging from

* Corresponding author. Tel.: +34 923 29 44 36; fax: +34 923 29 45 84.
  E-mail addresses: susan@usal.es (S. Sánchez-Orgaz), amd385@usal.es (A. Medina), anca@usal.es (A. Calvo Hernández).

Nomenclature

A_a	aperture area of the collector	α	effective emissivity
A_r	absorber area of the collector	η	overall efficiency
a_c	isentropic compressor pressure ratio	η_{max}	maximum overall efficiency with respect to the temperature ratio
a_t	isentropic turbine pressure ratio		
C	concentration ratio	$\eta_{max,max}$	maximum overall efficiency with respect to pressure and temperature ratios
C_w	heat capacity rate of the working fluid		
C_i	internal conductance of the power plant	η_s	efficiency of the solar collector
G	solar irradiance	η_h	thermal efficiency of the heat engine
$\dot{m}$	mass flow rate of the working substance	η_0	effective transmittance-absorptance product
M_1	radiation heat loss coefficient for the solar collector	ϵ_c	isentropic efficiency of the compressors
M_2	convection heat loss coefficient for the solar collector	ϵ_r	regenerator effectiveness
N_c	number of compressors	ϵ_t	isentropic efficiency of the turbines
N_t	number of turbines	ϵ_H	irreversibilities coming from the coupling of the working fluid with the heat reservoir at temperature T_H
$|\dot{Q}_H|$	heat-transfer rate between the working fluid and the heat reservoir at T_H		
$|\dot{Q}_L|$	heat-transfer rate between the working fluid and the heat reservoir at T_L	ϵ_L	irreversibilities coming from the coupling of the working fluid with the heat reservoir at temperature T_L
$|\dot{Q}_{HL}|$	heat-leak between heat reservoirs	γ	adiabatic coefficient
r_p	overall pressure ratio	ρ_H	irreversibilities due to pressure drops in the heat input
T_H	working temperature of the solar collector	ρ_L	irreversibilities due to pressure drops in the heat release
T_L	ambient temperature	σ	Stefan–Boltzmann constant
U_L	convective losses of the solar collector	τ	heat reservoirs temperature ratio
		ξ	heat leakage through the plant to the surroundings

---

one-compressor and one-turbine to two-compressors and two-turbines. For all the configurations we survey in this work, theoretical results for the optimized efficiencies, optimized collector temperatures, and optimized pressure ratios will be presented. We shall see that our predictions for the efficiency, obtained in the basis of a purely thermodynamic analytical framework, are in accordance with those of experimental prototypes. Moreover, the optimum values for temperature and pressure ratios are attainable with currently available technology.

Thermodynamic models like the one we have developed can contribute to improve the design and optimization of this kind of solar power plants in order to make them interesting from a commercial viewpoint. This kind of studies constitute a pre-design analysis with the aim to avoid losses and define the useful intervals of the basic parameters of the plant. Particularly, in this work we show the necessity of a global knowledge of the plant parameters to get an advantage from the use of a regenerator. Our model does not require details of the recuperator, the only relevant parameter is its effectiveness, so it applies to different recuperators built up from different technologies.

2. Numerical model

The plant scheme we shall analyze is depicted in Fig. 1 and the corresponding thermodynamic sketch in Fig. 2. The Brayton heat engine absorbs a net heat rate $|\dot{Q}_H|$ from the solar collector at temperature T_H and releases a net heat rate $|\dot{Q}_L|$ to the ambient at temperature T_L. We also assume a linear heat leakage, $|\dot{Q}_{HL}|$ directly from the hot reservoir at T_H to the cold heat sink at T_L [31].

As usual for a concentrating collector we consider that heat losses at low and intermediate temperatures are essentially associated to conduction and convection while at high enough temperatures radiation losses are dominant. In this model the useful energy delivered to the heat engine, $|\dot{Q}_H|$, and the efficiency of the solar collector η_s can be written, respectively, as [18,27,28,32]

$$|\dot{Q}_H| = \eta_0 G A_a - \alpha \sigma A_r T_L^4 (\tau^4 - 1) - U_L A_r T_L (\tau - 1), \quad (1)$$

$$\eta_s = \frac{|\dot{Q}_H|}{G A_a} = \eta_0 [1 - M_1 (\tau^4 - 1) - M_2 (\tau - 1)] \quad (2)$$

In these equations $\tau = T_H/T_L$ denotes the heat reservoirs temperature ratio, G is the solar irradiance, A_a and A_r are, respectively, the aperture and absorber areas, η_0 is the effective transmittance-absorptance product (optical efficiency). $M_1 = \alpha \sigma T_L^4/(\eta_0 GC), M_2 = U_L T_L/(\eta_0 GC)$, where U_L is the convective heat loss coefficient, α is the effective emissivity of the collector, $C = A_a/A_r$ is the concentration ratio, and σ the Stefan–Boltzmann constant. Indeed, if $M_2 = 0$ the model with purely radiative losses is recovered [26].

The model for the closed multi-step Brayton thermal cycle was reported recently. Here, we briefly summarize the most important steps in the thermodynamic cycle (see [29] for details):

(1) The working fluid, a constant mass flow of an ideal gas with constant heat capacities and adiabatic coefficient γ, is compressed from the initial state 1 by means of N_c non-adiabatic compressors and $N_c - 1$ isobaric intercoolers. All the compressors are assumed to have the same isentropic efficiency ϵ_c and the same inlet temperature T_1. In a recent study for a solarized Braysson cycle, Wu et al. [18] have evaluated the influence of temperature dependent heat capacities in the overall efficiency. They reported differences below 2% (Table 1 in [18]) in comparison with the case where the heat capacity remains constant. Thus, in order to obtain analytical expressions for heat input and heat release we assume constant heat capacities for the working fluid.

(2) After state 2 the gas is pre-heated to state X in a regenerative counterflow heat exchanger with effectiveness $\epsilon_r = (T_X - T_2)/(T_4 - T_2)$. A non-regenerative cycle corresponds to $\epsilon_r = 0$ while ideal or limit regeneration corresponds to $\epsilon_r = 1$. This interval of values for ϵ_r ensures that the temperature of the working fluid after the last compressor, T_2 is lower than that at the end of the expansions in the turbines, T_4 [33].

After X the working fluid is heated up to the final maximum temperature T_3. The global irreversibilities in this hot-end heat exchanger are accounted by $\epsilon_H = (T_X - T_3)/(T_X - T_H)$. The overall heating process from state 2 to 3 is considered as non-isobaric, with a pressure drop quantified by ρ_H ($\rho_H = 1$ corresponds to a zero pressure decay) [33,34].
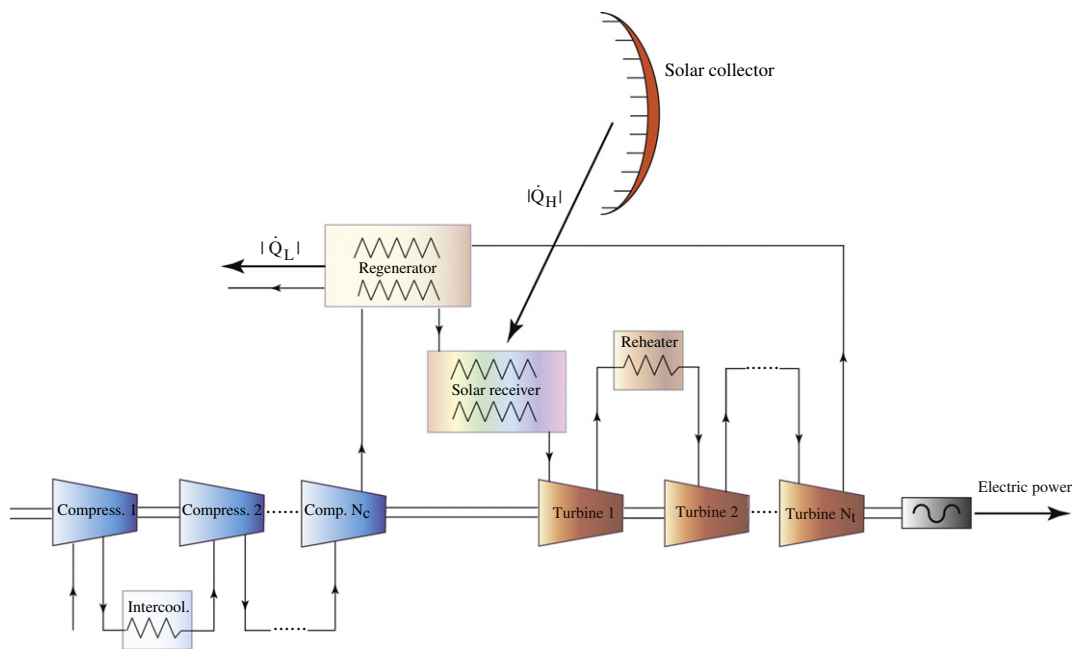
Fig. 1. Scheme of the solar-driven Brayton plant considered. It incorporates a recuperator and an arbitrary number of turbines and compressors and the corresponding intercoolers and reheaters.
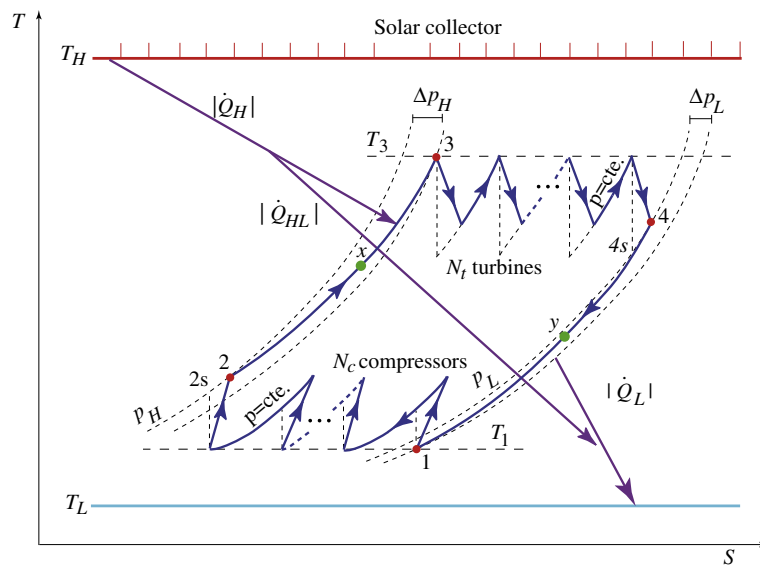

Fig. 2. T–S diagram of the thermodynamic cycle. Several irreversibility sources are considered (see text).

(3) From state 3 to 4 the working fluid is expanded by means of N_t non-adiabatic turbines and $N_t - 1$ isobaric reheaters. The efficiency of all turbines is the same, ϵ_t, and the inlet temperature for all of them is T_3.

(4) The exhaust process between 4 and 1 splits into two parts: a cooling from 4 to Y through a regenerative heat exchanger with effectiveness ϵ_r and a subsequent cooling from T_Y to T_1. $\epsilon_r = 0$ corresponds to $T_Y = T_4$ and $\epsilon_r = 1$ to $T_Y = T_2$. The effectiveness of this irreversible heat transfer is denoted as $\epsilon_L = (T_1 - T_Y)/(T_L - T_Y)$. A pressure decay is considered during the whole cooling process, which is quantified by ρ_L ($\rho_L = 1$ corresponds to a zero pressure decay) [34].

The basic mathematical equations of the model read as:

$$|\dot{Q}_H| = C_w T_L \left\{ \epsilon_H \left[\tau - Z_c(1 - \epsilon_r)\frac{T_1}{T_L} - \epsilon_r Z_t \frac{T_3}{T_L} \right] \right. $$
$$\left. + \epsilon_t(N_t - 1)(1 - a_t^{-1/N_t})\frac{T_3}{T_L} + \xi(\tau - 1) \right\}$$

$$|\dot{Q}_L| = C_w T_L \left\{ \epsilon_L \left[-1 + Z_t(1 - \epsilon_r)\frac{T_3}{T_L} + \epsilon_r Z_c \frac{T_1}{T_L} \right] \right. $$
$$\left. + \frac{1}{\epsilon_c}(N_c - 1)(a_c^{1/N_c} - 1)\frac{T_1}{T_L} + \xi(\tau - 1) \right\} \tag{4}$$

where C_w is the constant heat capacity rate of the working fluid, and

$$Z_c = 1 + \frac{a_c^{1/N_c} - 1}{\epsilon_c}$$
$$Z_t = 1 - \epsilon_t \left(1 - a_t^{-1/N_t}\right)$$

(5)

$$\frac{T_1}{T_L} = \frac{\epsilon_L + (1 - \epsilon_L)(1 - \epsilon_r)Z_t \left(\frac{T_3}{T_L}\right)}{1 - (1 - \epsilon_L)\epsilon_r Z_c}$$

(6)

$$\frac{T_3}{T_L} = \frac{\tau \epsilon_H [1 - (1 - \epsilon_L)\epsilon_r Z_c] + \epsilon_L (1 - \epsilon_H)(1 - \epsilon_r)Z_c}{[1 - (1 - \epsilon_L)\epsilon_r Z_c][1 - (1 - \epsilon_H)\epsilon_r Z_t] - (1 - \epsilon_H)(1 - \epsilon_L)(1 - \epsilon_r)^2 Z_t Z_c}$$

(7)

In these equations $a_t = a_c \rho_H \rho_L$, $a_c = T_{2s}/T_1 = r_p^{(\gamma-1)/\gamma}$ is the isentropic compressor pressure ratio, and $r_p = P_2/P_1$ the overall compression ratio. Finally, $\xi(\tau - 1) \equiv C_i/C_w(\tau - 1)$ accounts for the heat leakage $|\dot{Q}_{HL}|$ where C_i denotes the internal conductance of the power plant [31]. The interested reader can find the detailed obtention of Eqs. (3)–(7) in Ref. [29]. Here we just stress that in Eq. (3) the first term (proportional to ϵ_H) accounts for the heat provided to the system along the process $X \to 3$; the second one for the $(N_t - 1)$ reheating processes between turbines; and the third one for the heat transfer rate (heat-leak) through the plant. Similarly, in Eq. (4) the first term (proportional to ϵ_L) denotes the heat release along the path $Y \to 1$; the second one the heat transferred by the $(N_c - 1)$ intercoolers to the ambient; and the third one again is the heat leak.

Eqs. (3) and (4) for heat input and heat release, respectively, allow to obtain the efficiency of the Brayton heat engine, $\eta_h = |\dot{W}|/|\dot{Q}_H| = 1 - (|\dot{Q}_L|/|\dot{Q}_H|)$, where $|\dot{W}|$ is the net power output of the cycle. This thermal efficiency emerges as a function of the geometrical parameters that characterize the shape and size of the thermal cycle ($\tau = T_H/T_L, r_p = P_2/P_1, N_c, N_t$), of the parameters that quantify the internal irreversibilities ($\epsilon_t, \epsilon_c, \rho_H, \rho_L, \epsilon_r, \xi$), and of the parameters accounting for the external irreversibilities (ϵ_H, ϵ_L), i.e., the efficiency of the heat exchanger between the solar collector and the working fluid and that in the cold side between the gas and the surroundings.

This model for the multi-step Brayton heat engine was validated and compared with several real plants in [30,35]. We briefly detail the comparison with two particular experimental facilities. The predictions of the model for the commercial one-turbine one-compressor regenerative plant Turbec T100 [36,37] differ 2.7% for efficiency, 6.7% for the power output, and 4.2% for the heat input. When comparing with a two-compressors one-turbine regenerative plant [38,39], the model overestimates experimental efficiency by 2.8% and power output by 1.1%. These results show a satisfactory agreement of our Brayton multi-step theoretical model predictions with real plants. More details on the validation of our multi-step Brayton plant model can be found in [30,35].

The efficiency of the whole solar plant $\eta = |\dot{W}|/GA_a$ can be expressed as the product of the efficiency of the solar collector, $\eta_s(\rho_0, \tau, M_1, M_2)$ and that of the multi-step Brayton thermal heat engine $\eta_h(\tau, r_p, N_c, N_t, \epsilon_t, \epsilon_c, \rho_H, \rho_L, \epsilon_r, \xi, \epsilon_H, \epsilon_L)$:

$$\eta = \frac{|\dot{W}|}{GA_a} = \frac{|\dot{W}|}{|\dot{Q}_H|} \frac{|\dot{Q}_H|}{GA_a} \equiv \eta_h \eta_s$$

(8)

Hereafter, for the sake of simplicity in order to obtain numerical results, we shall take $\epsilon_t = \epsilon_c$, $\rho_H = \rho_L$ and $\epsilon_H = \epsilon_L \equiv \epsilon$.

3. Efficiency versus temperature ratio

The overall efficiency as a function of τ, $\eta(\tau)$, for the indicated configurations and three values of the pressure ratio ($r_p = 5, 15, 20$) is shown in Fig. 3. All irreversibility sources are con-
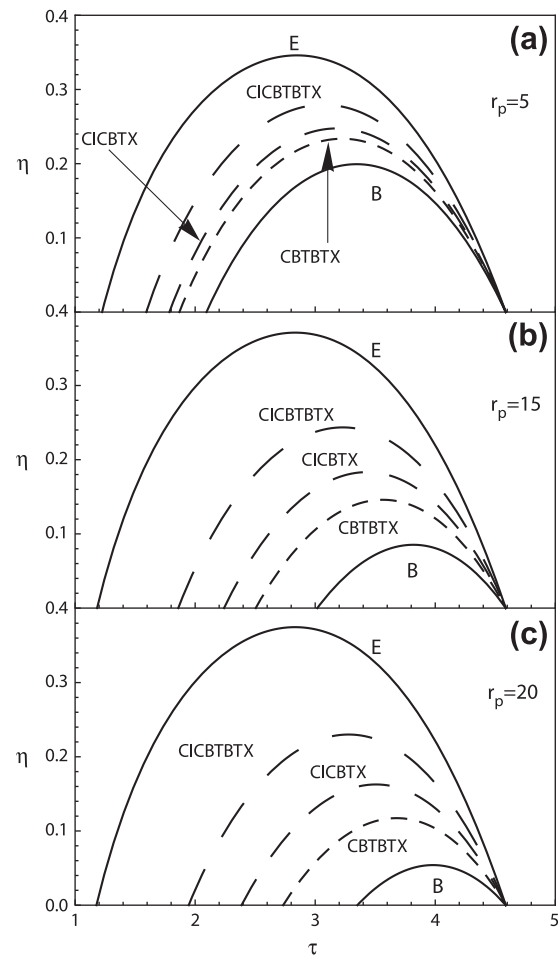

Fig. 3. Evolution of the overall plant efficiency with the external sources temperature ratio for the labeled plant configurations and different values of the pressure ratio: (a), $r_p = 5$; (b), $r_p = 15$, and (c), $r_p = 20$. The parameter values are (see Section 3): $\epsilon_t = \epsilon_c = 0.95$, $\rho_H = \rho_L = 0.98$, $\epsilon_r = 0.95$, $\epsilon_H = \epsilon_L \equiv \epsilon = 0.90$, $\xi = 0.02$, $T_L = 300K$, $\gamma = 1.4$, $\eta_0 = 0.80$, $M_1 = 2.25 \times 10^{-3}$, and $M_2 = 1.5 \times 10^{-3}$.

sidered together with realistic values [29,34,40–42]: $\epsilon_t = \epsilon_c = 0.95$, $\rho_H = \rho_L = 0.98$, $\epsilon_r = 0.95$, and $\epsilon = 0.90$, $\xi = 0.02$, $T_L = 300$ K, $\gamma = 1.4$. Parameters for the solar collector are [18,26]: $\eta_0 = 0.80$, $M_1 = 2.25 \times 10^{-3}$, and $M_2 = 1.5 \times 10^{-3}$. We have checked that small (reasonable) variations on any of these parameters do not alter the shape of the curves we show in this section and in the following ones nor the conclusions of this work.

Following Horlock's notation [43], CICIC···BTBT···X denotes an arrangement with several compressors (C) and intermediate intercoolers (I), several turbines (T) and intermediate reheaters (B), and regeneration (X). So, CBTX represents a simple Brayton cycle with regeneration, hereafter B arrangement; CICBTX stands for two compressors with intermediate intercooling and one turbine; CBTBTX for one compressor and two turbines with intermediate reheating; and CICBTBTX for two compressors and two turbines with intermediate intercooling and reheating. An Ericsson-like solar plant model (E-configuration) emerges when $N_t = N_c \to \infty$. All configurations, at any value of the pressure ratio, display a parabolic-shaped overall efficiency. The range for the temperature ratios that lead to positive efficiencies, for each configuration, decreases as r_p increases. It should be also noted that the overall efficiency of the considered configurations shows an optimum maximum value at a given temperature ratio. A closer inspection of the Fig. 3 shows that: (a) for the r_p-values presented, the maximum efficiency for each configuration decreases as r_p increases; (b) at any pressure ratio the maximum efficiency values decrease in

the sequence E, CICBTBTX, CICBTX, CBTBTX, B while the corresponding τ-values increase. From a thermodynamic point of view, all these behaviors are a straight consequence of the coupling between the solar collector and the pure thermal device. In fact, the efficiency of the corresponding non-solar Brayton configurations presents a monotonic behavior with the temperature ratio as we shall see below in Section 4 and in the insets of Fig. 6.

At sight of the results in Fig. 3 one could expect that in order to obtain higher overall efficiencies and smaller temperatures in the collector a reduction of pressure ratios would be desirable (see, for example [44]). However this is not true in all cases, as it is shown in Fig. 4. In this figure the resulting optimized efficiencies $\eta_{max}(r_p)$ (Fig. 4a) and the corresponding $\tau_{max}(r_p)$ (Fig. 4b) in terms of r_p are plotted. These figures show that for high enough pressure ratios, $\eta_{max}(r_p)$ is a decreasing function of r_p for all the analyzed configurations (except the theoretical upper limit given by the E-configuration) while $\tau_{max}(r_p)$ shows an increasing behavior. Nevertheless, the opposite behavior appears when r_p is small enough for all configurations except E: maximum efficiency increases as r_p increases while the corresponding τ decreases. Physically the most relevant issue from results in Fig. 4 is that $\eta_{max}(r_p)$ shows a well-defined maximum for small pressure ratios, whereas the temperature ratio $\tau_{max}(r_p)$ shows a well-defined minimum. As it will be detailed in Section 5, the first of these facts allows for a double optimization of η with respect to τ and r_p. Before, we analyze in the next section the evolution of this optimized efficiency $\eta_{max}(r_p)$ with ϵ_r, the parameter which accounts for the efficiency of the regeneration process.

4. Optimized efficiency versus regenerator effectiveness

Let us consider the most simple configuration of a regenerative solar-driven Brayton cycle ($N_t = N_c = 1$). In Fig. 5 we plot $\eta_{max}(\epsilon_r)$ for several values of the pressure ratio, $r_p = 5$, 15, and 20 and three values of ϵ between 0.75 and 1.0. For all the other parameters the same values that in Fig. 3 are considered. The figure shows that
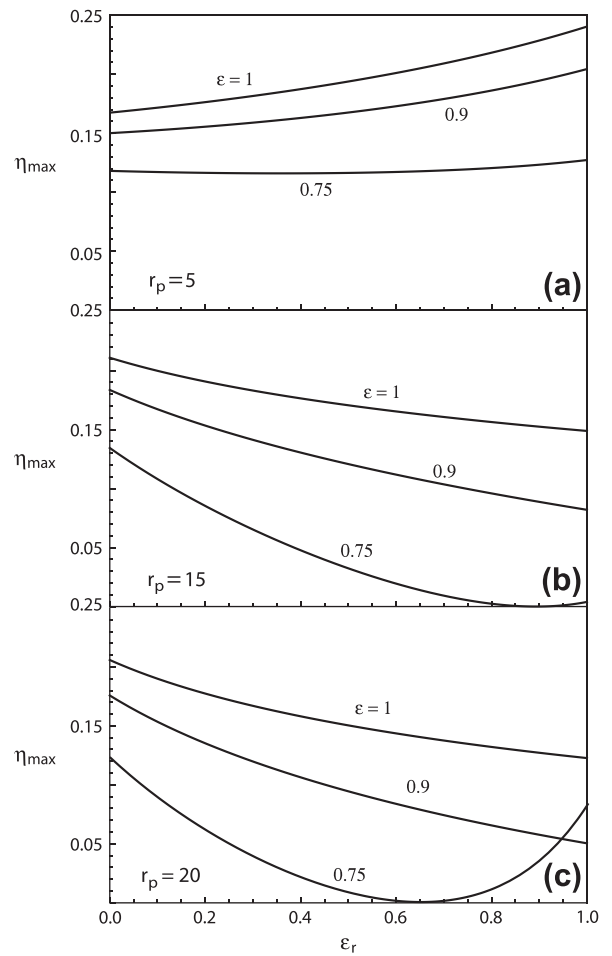
Fig. 5. Dependence of the optimum maximum efficiency η_{max} for a simple solar Brayton arrangement with the parameter ϵ_r accounting for the irreversibilities in the recuperator. $\epsilon_r = 1$ corresponds to a perfect regenerator and $\epsilon_r = 0$ corresponds to the non-recuperative situation. For each value of r_p three curves are presented in terms of the efficiency ϵ of the external heat exchangers, $\epsilon = 1$ (ideal exchangers), 0.9 and 0.75. Remainder parameters are the same as in Fig. 3.

only for small values of the pressure ratio, maximum efficiency increases with the regenerator effectiveness. Even for small r_p, if the irreversibilities arising from the coupling of the thermal engine with the heat reservoirs are large ($\epsilon \lesssim 0.75$), η_{max} is a decreasing function of ϵ_r. As r_p becomes larger the decreasing is steeper. For large r_p values and high losses in the coupling with the heat reservoirs, η_{max}, presents a minimum and thereafter increases with ϵ_r. It has been checked that, for the parameters considered, the change of behavior happens between $r_p = 5$ and 8: smaller r_p values lead to increasing $\eta_{max}(\epsilon_r)$ and larger r_p values result in a loss of maximum efficiency when raising up the recuperator effectiveness.

These results show that in a solarized simple Brayton cycle the interplay between efficiency and regeneration is quite more complex than in a Brayton cycle working alone, where high thermal efficiency is accomplished by high regeneration at small pressure ratios. In fact, for the solar-driven case if pressure ratios are high enough and/or external coupling irreversibilities are significant, a large value in the recuperator effectiveness could result in a decreasing of efficiency for the plant. In order to get a physical explanation of this fact we plot in Fig. 6 the overall efficiency η for a one-turbine one-compressor Brayton regenerative solar-driven engine ($N_t = N_c = 1$), as a function of τ for the same values of the pressure ratio, $r_p = 5$, 15, and 20 and the indicated values of ϵ_r. The corresponding insets in the figure show the efficiency of the thermal heat engine working alone, η_h and the behavior of
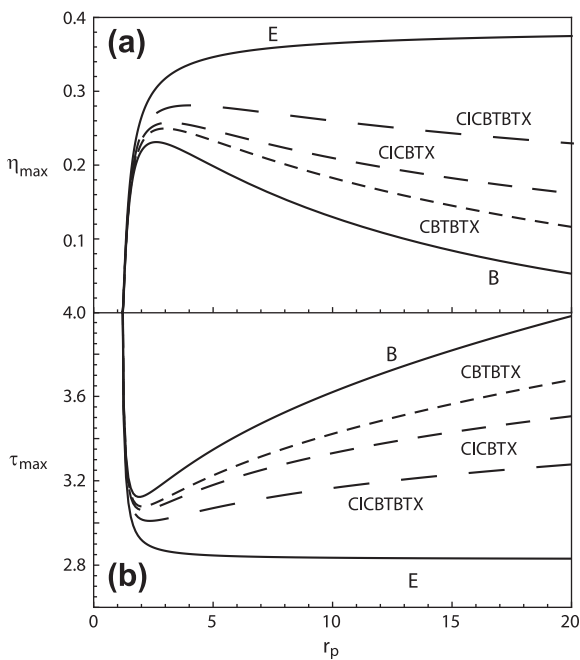

Fig. 4. (a) Evolution with the pressure ratio of the maximum overall efficiency η_{max} when optimized with respect to the temperature ratio τ. (b) Evolution with the pressure ratio of the optimum temperature ratio τ_{max}. Parameters are the same as in Fig. 3.
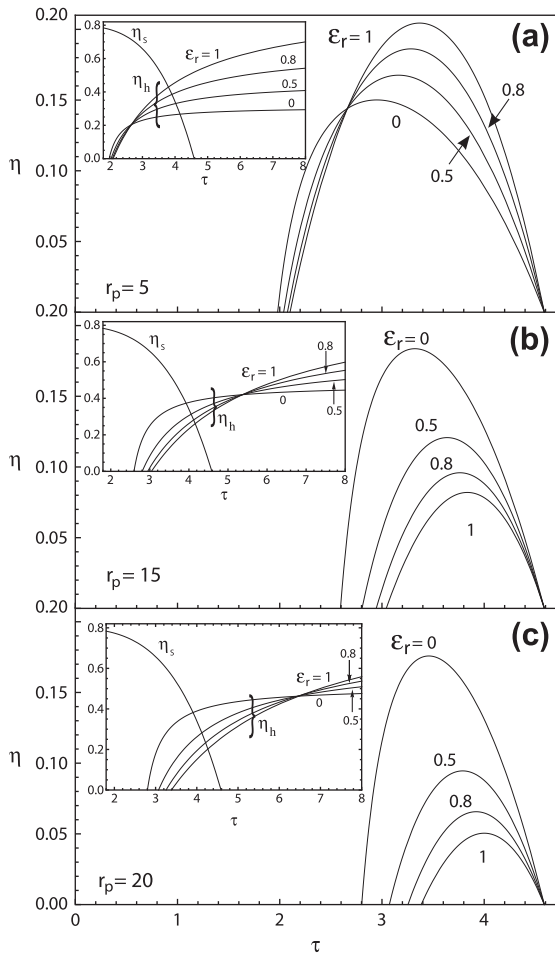
Fig. 6. Behaviour of the overall efficiency η for a simple solar Brayton arrangement with the temperature ratio τ in terms of the effectivenes recuperator ϵ_r for the shown values of r_p. The corresponding insets show the corresponding behavior of the solar collector efficiency η_s and of the thermal part η_h (see Eq. (8)). Remainder parameters are the same as in Fig. 3.

the efficiency of the solar collector with τ given by Eq. (2). Accordingly, $\eta_s = \eta_s(\tau; \eta_0, M_1, M_2)$, is a monotonic decreasing function of τ for whichever value of the losses coefficients M_1 and M_2. Opposite, $\eta_h(\epsilon_r)$, increases with the temperature ratio, so the overall efficiency is always a parabolic function of τ. Note in the insets how the intersections of η_s with the curves $\eta_h(r_p, \epsilon_r)$ are in the decreasing order of ϵ_r at small pressure ratios (inset of Fig. 6a) but at high pressure ratios the intersections are in a increasing order with ϵ_r (insets of Fig. 6b and c). As a consequence, for enough small pressure ratios ($r_p = 5$, Fig. 6a) the largest overall efficiency η is obtained for $\epsilon_r = 1$ and the lowest is obtained in the absence of recuperator. On the contrary, for intermediate and high r_p values ($r_p = 15, 20$; Fig. 6b and c) an ideal recuperator gives the poorest overall efficiency. The width of the temperature ratio intervals giving positive efficiencies narrows with increasing r_p, shifts to the right, and also the values of τ giving the maximum of that parabolic shaped curves become higher. In summary, in a simple irreversible Brayton solar-driven engine an efficient recuperator ensures an increasing of the maximum overall efficiency only for small enough pressure ratios, according to the results in Fig. 5.

We have repeated the calculations of the overall system efficiency considering the same parameters that in the previous sections, for several combinations of N_t and N_c up to 2 that could be a reasonable limit because of practical and economical considerations [45]. For the arrangements CBTBTX or CICBTX the maximum

efficiency as a function of ϵ_r presents an aspect very similar to the simple one-turbine one-compressor Brayton system, i.e., that of Fig. 5. It is necessary to consider at least an arrangement with two turbines and two compressors CICBTBTX to get increasing functions for $\eta_{\max}(\epsilon_r)$ for a wide interval of pressure ratios. This is depicted in Fig. 7. At small pressure ratios (Fig. 7a), this configuration shows a monotonically increasing behavior with ϵ_r for any value of ϵ. For $r_p = 15$, $\eta_{\max}$ also increases but more slowly. For $r_p = 20$, curves become flatter, so $\eta_{\max}$ is almost independent of ϵ_r.

In Fig. 7 it is also included the limit case where the number and turbines and compressors trends to infinity ($N_t, N_c \to \infty$), that would represent an Ericsson solar-driven engine. For this particular case maximum efficiency always has an appreciable increase with ϵ_r, for any value of ϵ. With limit regeneration, $\epsilon_r = 1$, all the curves collapse to a unique value of $\eta_{\max}$, independent of ϵ. Any other configuration, with a number of turbines and compressors over 2 would lead to maximum efficiencies in the region between the curves corresponding to ($N_t = 2, N_c = 2$) and the Ericsson limit.

The insets in Fig. 6 also allow to explain the narrowing of the effective interval of values of τ that give positive overall efficiencies, as we commented from Fig. 3. The upper limit comes from η_s, i.e., from the solar collector, so it only depends on its characteristics (optical efficiency, concentration ratio, heat transfer losses and so on) and it is independent of r_p, a parameter of the turbine.
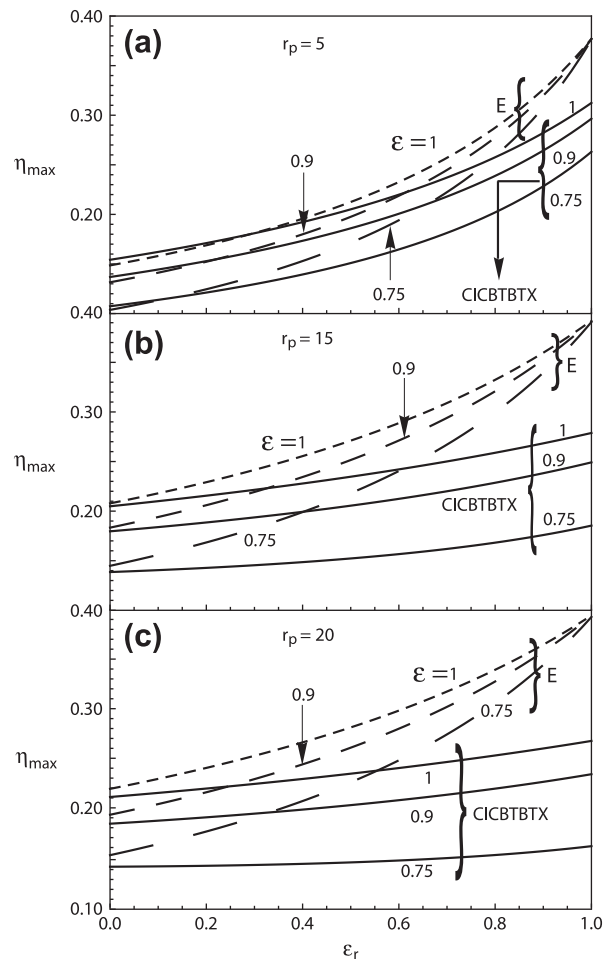

Fig. 7. Dependence with ϵ_r of the optimum maximum efficiency $\eta_{\max}$ for a solar Brayton arrangement with two compressors and two turbines. For each pressure ratio curves are presented for three values of the efficiency ϵ of the external heat exchangers, $\epsilon = 1$ (ideal exchangers), 0.9 and 0.75. In each case the theoretical upper limit given by the solar Ericsson cycle is also shown. Remainder parameters are the same as in Fig. 3.

For the parameters we elected the upper limit is around $\tau = 4.6$. On the contrary, the lower limit comes from the characteristics of the gas turbine. It depends at least on ϵ_r and r_p as it is observed in the insets of Fig. 6. Particularly, it displaces to higher values when r_p increases. Thus, when the pressure ratio is increased the upper value of τ keeps constant, and the lower one displaces to the right. In consequence the overall efficiency, $\eta = \eta_h \eta_s$, has an effective useful interval for τ that narrows with increasing r_p. So, the thermodynamic explanation of this narrowing should be ascribed to the interplay between both systems, the solar collector and the gas turbine.

5. Double optimization procedure

As it is shown in Fig. 4, the overall efficiency considered as a function of the pressure and the temperature ratios, $\eta = \eta(r_p, \tau) = \eta(r_p, \tau) = \eta_s(\tau)\eta_h(r_p, \tau)$ admits a double and simultaneous optimization with respect to r_p and τ. Here, we deal with the influence of the regenerator effectiveness on the double optimized overall efficiency, that we shall denote as $\eta_{max,max}$. This is depicted in Fig. 8a. In any case it is observed that $\eta_{max,max}$ increases as it does ϵ_r. This means that if in the plant design the pressure ratio and the working temperature of the solar collector are simultaneously chosen to be close to those values maximizing the overall efficiency, an investment to improve regenerator effectiveness always improve net efficiency. Another point shown by Fig. 8a is that the slope of the

Fig. 8. Dependence with ϵ_r for the labeled solar Brayton arrangements of: (a) the double optimized overall efficiency $\eta_{max,max}$; (b) the optimized pressure ratios $r_{p_{max,max}}$; and (c) the optimized temperature ratios $\tau_{max,max}$. Parameters are the same as in Fig. 3.

increasing of $\eta_{max,max}$ is similar for all the configurations considered.

Fig. 8b and c shows the evolution with ϵ_r of the values of the pressure ratio $r_{p_{max,max}}$ and the temperature ratio $\tau_{max,max}$ giving the maximum efficiency. Optimum pressure ratios decrease with ϵ_r, but its downtrend strongly depends on the plant configuration elected and it is faster as the number of turbines and compressors in the plant configuration increases. The optimized temperature ratio, $\tau_{max,max}$, also decreases for all configurations with ϵ_r but now with an almost constant decay.

A different election of the values of the parameters (both for the solar collector as well as for the thermal device) could give different numerical values of the optimized magnitudes. However, we have checked that all plotted behaviors and conclusions along the paper remain unchanged. Comparison between calculated results and experimental ones is a quite complex task mainly due to the difficulty to obtain from the experimental literature the correct values of the parameters required in our calculations, specially those accounting for the external coupling of the thermal power plant. Nevertheless, with the set of parameters considered up to now and realistic values of regeneration, say $\epsilon_r = 0.9$, the calculated double-optimized efficiencies are in the range between 0.21 for the B configuration and 0.26 for the configuration with two turbines and two compressors and the required optimized pressure ratios are in the range between 3 and 5, respectively. The optimized temperatures in the solar collector lies between 918 K for the simple Brayton solar arrangement and 950 K for the configuration with two turbines and two compressors (for an ambient temperature of 300 K). These optimized theoretical values are amenable to be roughly compared with some solar-hybrid gas turbine prototype plants working with pressurized air receivers when the additional fossil fuel combustor is not considered: The Heron H1 unit (intercooled recuperated two-shaft engine) and the Solar Mercury 50 unit (recuperated single shaft gas turbine) [4]; the solarized Brayton one-compressor and two-turbines plant with DLR receiver reported in [1] and even with results for alternative cycles based on carbon dioxide for central receivers: a stand-alone closed recuperative, simple Brayton topping cycle (layout 1 in [6]) and two-stage compression cycle (layout 2 in [6]).

Our model is capable to give a precise interval for the main thermodynamic parameters of the solar-driven plant in order to design it in conditions close to the obtention of the maximum overall efficiency. Moreover, the model is independent of the peculiarities of the recuperator or the other basic elements of the plant: heat exchangers, turbines and compressors, etc. Only a gross estimation of their efficiencies is required. The final design of the plant should incorporate such peculiarities through a pertinent economic or thermoeconomic analysis including the possibility of performance regimes based on different optimization criteria [21,31,46–49].

6. Summary and conclusions

We have presented an analysis on the influence of the regenerator effectiveness in a multi-step solarized Brayton cycle model. For the thermal cycle the model assumes a regenerative multi-step Brayton heat engine with an arbitrary number of turbines and compressors, and the main irreversibility sources in this kind of power plants: the non-ideal behavior of turbines and compressors, pressure drops in the heat input and heat release, regenerator irreversibility, heat leakage through the plant to the surroundings, and non-ideal couplings of the working fluid with the external heat reservoirs. The solar collector is considered with heat losses proportional both to τ^4 and τ terms.

The analytical optimization process developed in this work is based on the parabolic-shaped behavior of the overall efficiency
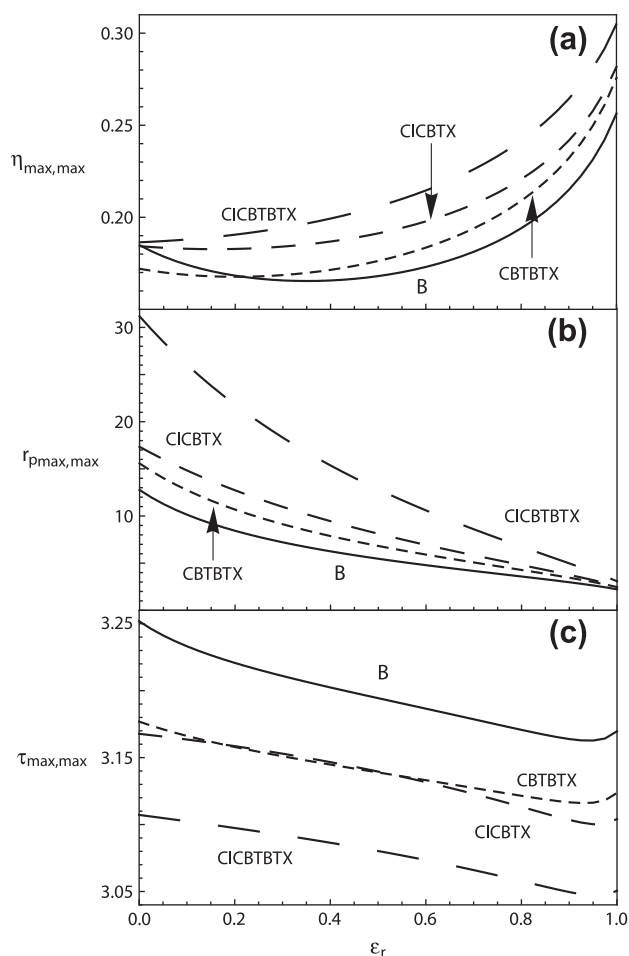
with the temperature ratio for any value of the pressure ratio, which is a direct consequence of the coupling of the thermal multi-step Brayton cycle with the solar collector. Moreover, an additional optimization can be obtained in terms of the pressure ratio. For a realistic set of the values accounting for the different irreversibility sources, the resulting optimized pressure ratio and collector temperature as well as the double optimized efficiency are comparable with reported results for solarized gas turbine power plants.

As main results we stress the following points. First, for a simple Brayton engine coupled to a concentrating solar collector, an increase of the regeneration effectiveness does not necessarily lead to an improvement in the overall efficiency. This is true only for small pressure ratios. Second, the problem can be avoided with a configuration for the Brayton engine with two turbines and two compressors. Third, for any plant arrangement (including the simplest one-turbine one-compressor) the election of the values of τ and r_p that lead to a double maximized efficiency ensures that an improvement in recuperator effectiveness always leads to an increase in the overall efficiency of the plant.

Thus, our numerical model could be elucidating in the design and optimization of realistic solarized, multi-step gas turbine power plants. In particular, the introduction of a regenerator (i.e., the reduction of the surface of the concentration system and a saving of investment and maintenance costs) should be accomplished with a detailed plant design on the pressure ratio and the working temperature of the solar collector, which could be elected simultaneously to be close to those values maximizing the overall efficiency.

Acknowledgement

References

[1] D. Gallup, J. Kesseli, A solarized Brayton engine based on turbo-charger technology and the DLR receiver. In: Proceedings of the IECEC-AIAA-94-3945, Monterrey, CA, 1994.

[2] Kribus A. A high-efficiency triple cycle for solar power generation. Solar Energy 2002;72:1–11.

[3] J. Sinai, C. Sugarmen, U. Fisher, Adaptation and modification of gas turbines for solar energy applications. In: Proceedings of GT2005 ASME Turbo Expo 2005, 2005.

[4] Schwarzbözl P, Buck R, Sugarmen C, Ring A, Marcos Crespo M, Altwegg P, et al. Solar gas turbine systems: design, cost and perspectives. Solar Energy 2006;80:1231–40.

[5] Heller P, Pfänder M, Denk T, Tellez F, Valverde A, Fernandez J, et al. Test and evaluation of a solar powered gas turbine system. Solar Energy 2006;80:1225–30.

[6] Chacartegui R, Muñoz de Escalona J, Sánchez D, Monje B, Sánchez T. Alternative cycles based on carbon dioxide for central receiver solar power. Appl Thermal Eng 2011;31:872–9.

[7] Segal A, Epstein M. Comparative performances of 'tower-top' and 'tower-reflector' central solar receivers. Solar Energy 1999;65:207–26.

[8] Ávila-Marín A. Volumetric receivers in solar thermal power plants with centra receiver system technology: a review. Solar Energy 2011;85:891–910.

[9] Sahin A. Optimum operating conditions of solar-driven heat engines. Energy Convers Manage 2000;41:1335–43.

[10] Koyun A. Performance analysis of a solar-driven heat engine with external irreversibilities under maximum power and power density condition. Energy Convers Manage 2004;45:1941–7.

[11] Barranco-Jiménez M, Sánchez-Salas N, Rosales MA. Thermoeconomic optimum operation conditions of a solar-driven heat engine model. Entropy 2009;11:443–53.

[12] McGovern R, Smith W. Optimal concentration and temperatures of solar thermal power plants. Energy Convers Manage 2012;60:226–32.

[13] Salah El-Din M. Thermodynamic optimisation of irreversible solar heat engines. Renew Energy 1999;17:183–90.

[14] Göktun S. Finite-time optimization of a solar-driven heat engine. Solar Energy 1996;56:617–20.

[15] Zhang Y, Lin B, Chen J. The unified cycle model of a class of solar-driven heat engines and their optimum performance characteristics. J Appl Phys 2005;97:084905.

[16] Yilmaz T, Ust Y, Erdil A. Optimum operating conditions of irreversible solar driven heat engines. Renew Energy 2006;31:1333–42.

[17] Zheng S, Chen J, Lin G. Performance characteristics of an irreversible solar-driven Braysson heat engine at maximum efficiency. Renew Energy 2005;30:601–10.

[18] Wu L, Lin G, Chen J. Parametric optimization of a solar-driven Braysson heat engine with variable heat capacity of the working fluid and radiation–convection heat losses. Renew Energy 2010;35:95–100.

[19] Blank D, Wu C. Finite-time power limit for solar-radiant Ericsson engines in space applications. Appl Therm Eng 1998;18:1347–57.

[20] Sogut OS, Durmayaz A. Performance optimization of a solar-driven heat engine with finite-rate heat transfer. Renew Energy 2005;30:1329–44.

[21] Sahin B, Ust Y, Yilmaz T, Akcay IH. Thermoeconomic analysis of a solar driving heat engine. Renew Energy 2006;31:1033–42.

[22] Gandhidasan P. Thermodynamic analysis of a closed-cycle, solar gas-turbine plant. Energy Convers Manage 1993;34:657–61.

[23] le Roux W, Bello-Ochende T, Meyer J. Operating conditions of an open and direct solar thermal Brayton cycle with optimised cavity receiver and recuperator. Energy 2011;36:6027–36.

[24] le Roux W, Bello-Ochende T, Meyer J. Thermodynamic optimisation of the integrated design of a small-scale solar thermal Brayton cycle. Int J Energy Res 2012;36:1088–104.

[25] Zhang Y, Lin B, Chen J. Optimum performance characteristics off an irreversible solar-driven Brayton heat engine at the maximum overall efficiency. Renew Energy 2007;32:856–67.

[26] Fraidenraich N, Gordon J, Tiba C. Optimization of gas-turbine combined cycles for solar energy and alternative-fuel power generation. Solar Energy 1992;48:301–7.

[27] Bejan A. Advanced engineering thermodynamics. 3rd ed. Hoboken (NJ): Wiley; 2006.

[28] Duffie J, Beckman W. Solar engineering of thermal processes. Hoboken (NJ): John Wiley and Sons; 2006.

[29] Sánchez-Orgaz S, Medina A, Calvo Hernández A. Thermodynamic model and optimization of a multi-step irreversible Brayton cycle. Energy Convers Manage 2010;51:2134–43.

[30] Sánchez-Orgaz S, Medina A, Calvo Hernández A. Maximum overall efficiency for a solar-driven gas turbine power plants. Int J Energy Res. http://dx.doi.org/10.1002/er.2967.

[31] Ust Y. Effects of combined heat transfer on the thermo-economic performance of irreversible solar-driven heat engines. Renew Energy 2007;32:2085–95.

[32] Xie W, Dai Y, Wang R. Numerical and experimental analysis of a point focus solar collector using high concentration imaging PMMA Fresnel lens. Energy Convers Manage 2011;52:2417–26.

[33] Calvo Hernández A, Medina A, Roco JMM. Power and efficiency in a regenerative gas turbine. J Phys D: Appl Phys 1995;28:2020–3.

[34] Roco JMM, Velasco S, Medina A, Calvo Hernández A. Optimum performance of a regenerative Brayton thermal cycle. J Appl Phys 1997;82:2735–41.

[35] Sánchez-Orgaz S. Modelization, analysis, and thermodynamic optimization of Brayton multi-step power plants. solar applications. Ph.D. Thesis, Universidad de Salamanca, Spain, 2012.

[36] Sunden B. High temperature heat exchangers (HTHE). In: Proceedings of the fifth international conference on enhanced, compact and ultra-compact heat exchangers: science, engineering and technology, Hoboken, NJ, USA, 2005.

[37] Kautz M, Hansen U. The externally fired gas turbine (EFGT-cycle) and simulation of the key components. Appl Energy 2007;84:795–805.

[38] Romier A. Small gas turbine technology. Appl Thermal Eng 2004;24:1709–23.

[39] EU Project. Coordinator: Microturbo S.A. (France). Research and development of high efficiency components for an intercooled, recuperated CHP gas turbine for combined heat and efficient power. Tech rep, Comunidad Europea, Contract No. ENK5-CT-2000-00070 (2000–2003).

[40] Medina A, Roco JMM, Calvo Hernández A. Regenerative gas turbines at maximum power density conditions. J Phys D: Appl Phys 1996;29:2802–5.

[41] Chen L, Wang J, Sun F. Power density analysis and optimization of an irreversible closed intercooled regenerated Brayton cycle. Math Comput Model 2008;48:527–40.

[42] Herrera C, Sandoval J, Rosillo M. Power and entropy generation of an extended irreversible Brayton cycle: optimal parameters and performance. J Phys D 2006;39:3414–24.

[43] Horlock J. Advanced gas turbine cycles. Oxford: Pergamon; 2003.

[44] Cengel Y, Boles M. Thermodynamics: an engineering approach. 6th ed. McGraw-Hill; 2007.

[45] Horlock J. Cogeneration-combined heat and power plants. Krieger; 1997.

[46] Sogut OS, Ust Y, Sahin B. The effects of intercooling and regeneration on the thermo-ecological performance analysis of an irreversible-closed Brayton heat engine with variable temperature thermal reservoirs. J Phys D: Appl Phys 2006;39:4713–21.

[47] Ust Y, Sahin B, Kodal A, Akcay IH. Ecological coefficient of performance analysis and optimization of an irreversible regenerative-Brayton heat engine. Appl Energy 2006;83:558–72.

[48] Ust Y, Sogut OS, Sahin B, Durmayaz A. Ecological coefficient of performance (ECOP) optimization for an irreversible heat engine with variable-temperature heat reservoirs. J Energy Inst 2006;79:47–52.

[49] Ust Y, Sahin B, Kodal A. Performance analysis of an irreversible Brayton heat engine based on ecological coefficient of performance criterion. Int J Thermal Sci 2006;45:94–101.